ChemComm

COMMUNICATION

View Article Online
View Journal | View Issue

Cite this: *Chem. Commun.*, 2024, **60**, 14806

Received 7th August 2024,
Accepted 18th November 2024

DOI: 10.1039/d4cc04021j

rsc.li/chemcomm

Broadband emission in alkali halides triggered by Sb^{3+} doping†

Yanyan Li,[ab] Mircea Cotlet,[c] Ido Hadar[d] and Peijun Guo *[ab]

Broadband emission in a series of alkali chlorides are achieved by doping NaCl, KCl, and RbCl with Sb^{3+}. These compounds show photoluminescence peaks in the visible range of 536–574 nm with long lifetimes in the microsecond range. Our findings could offer valuable insights for the development of new lead-free phosphors.

Luminescent metal halide perovskites have attracted significant research attention due to their distinctive properties and various potential applications in optoelectronics including light-emitting diodes (LEDs),[1–3] solar cells,[4–6] photodetectors,[7,8] and scintillators.[9,10] However, their practical applications are hindered by the presence of toxic lead and material instability. Therefore, considerable efforts have been devoted to the development of new types of lead-free metal halides with superior properties and environmental friendliness. These include homovalent replacements of Pb using Sn or Ge,[11,12] heterovalent substitutions with Bi and Sb,[13,14] combinations of monovalent and trivalent elements to create lead-free double perovskites,[15] and copper-based perovskite derivatives.[16]

The incorporation of metal-ion dopants into metal halides has proven to be an effective strategy for regulating band structures or introducing new luminescence centers in these materials.[17–20] Sb^{3+}-doped metal halides, in particular, have gained significant attention due to their low toxicity and efficient emission properties. Sb^{3+} plays a crucial role in the energy band and the excited state modulation of the matrix materials. For instance, doping $[NH_3(CH_2)_4NH_3]CdBr_4$ perovskite with Sb^{3+} facilitates efficient exciton transfer, resulting in efficient triplet Sb^{3+} emission with a photoluminescence (PL) peak at 640 nm and near-unity photoluminescence quantum yield (PLQY).[21] Xia's group demonstrated that incorporating Sb^{3+} in $Cs_2InCl_5 \cdot H_2O$:Sb^{3+} yielded broad yellow luminescence with a high efficiency of 95.5%. Similarly, Chang *et al.* synthesized 3D double perovskites $Sb:Cs_2KInCl_6$ *via* a solvothermal method, achieving green emission with a PLQY of up to 99.2%.[22] Additionally, the PLQY of $InCl_6(C_4H_{10}SN)_4 \cdot Cl$ was significantly enhanced from 20% to 90% by the Sb^{3+} doping.[23] Inspired by the remarkable improvement in optical properties through Sb^{3+} doping, here we apply this strategy to a new class of metal halides.

Sodium chloride (NaCl) as an earth-abundant material is essential for both everyday life and industrial processes. Its extensive availability, affordability, and versatility highlight its significance across various sectors, establishing it as a key material with promising potential for innovative applications. The natural NaCl has been reported to exhibit thermoluminescence (TL), infrared stimulated luminescence (IRSL) and radioluminescence (RL) under X-ray irradiation.[24] Similar to the classic thallium-doped NaI used in scintillators,[25,26] NaCl can also accommodate doping with various ions.[27] For example, Eu^{2+}-doped NaCl exhibits TL under ultraviolet (UV), x-, β- and α-ray irradiation, making it suitable for X-radiation dosimeters.[28] NaCl:Ce^{3+} shows UV emission at 342 nm when excited at 267 nm,[27] and Pb^{2+}-doped NaCl displays two bands, a low-energy band at 3.26 eV and a high-energy band at 3.94 eV.[28] To the best of our knowledge, while Sb^{3+} and Sb^{2+} impurities in NaCl produce optical absorption bands at 268 nm and 212 nm, no visible light emission from ion-doped NaCl has been reported.[29]

In this work, we successfully doped Sb^{3+} into NaCl. This synthesis strategy can also be extended to KCl and RbCl. The obtained Sb^{3+}-doped alkali chlorides ACl (A = Na, K, and Rb) exhibit broadband green to yellow light emission attributable to self-trapped excitons (STEs). Our work presents a straightforward doping strategy to tune the optical performance of non-toxic materials, providing insights into the development of new materials for optoelectronic applications.

[a] *Department of Chemical and Environmental Engineering, Yale University, 9 Hillhouse Avenue, New Haven, CT 06520, USA. E-mail: peijun.guo@yale.edu*
[b] *Energy Sciences Institute, Yale University, 810 West Campus Drive, West Haven, CT 06516, USA*
[c] *Center for Functional Nanomaterials, Brookhaven National Laboratory, Upton, NY 11973, USA*
[d] *Institute of Chemistry, and the Center for Nanoscience and Nanotechnology, The Hebrew University of Jerusalem, Jerusalem, 91904, Israel*

† Electronic supplementary information (ESI) available: Experimental details and various characterizations. See DOI: https://doi.org/10.1039/d4cc04021j

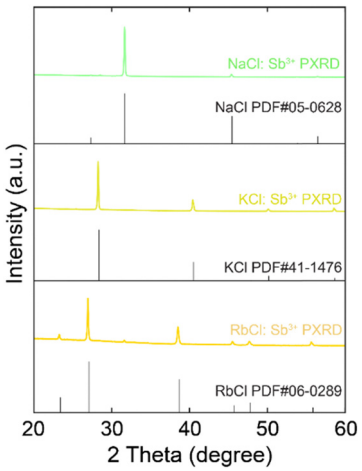

Fig. 1 PXRD pattern of Sb^{3+}-doped ACl (A = Na, K, and Rb) single crystals compared to standard XRD patterns PDF# 05-0628 of NaCl, PDF# 41-1476 of KCl, and PDF# 06-0289 of RbCl.

Sb^{3+}-doped NaCl single crystals (SCs) were first synthesized using the slow evaporation method. The nominal concentration of Sb^{3+} dopant was controlled by varying the stoichiometry of SbCl/NaCl in the precursor (experimental details in the ESI†). The as-synthesized NaCl:Sb^{3+} SCs retain the cubic $Fm\bar{3}m$ symmetry (similar to the undoped compound), as their powder X-ray diffraction (PXRD) patterns (Fig. 1) match well with the standard XRD pattern (PDF# 05-0628) of NaCl with no observable extra peaks resulting from the incorporation of Sb^{3+} ions. The slight shift of diffraction peaks towards lower angles after doping may be caused by the electronegativity differences and the expansion of cell volume induced by the Sb^{3+} dopants. Fig. S1 (ESI†) shows a typical scanning electron microscopy (SEM) and an energy dispersive spectroscopy (EDS) elemental map of the NaCl:Sb^{3+} crystals. The results confirm the presence of Na, Cl, and Sb in the sample, and demonstrates that these elements are homogeneously distributed within the crystals.

The as-synthesized 30% (nominal) Sb^{3+}-doped NaCl crystals have a lateral size of 2–3 mm and are transparent under room light, indicating no absorption in the visible range. The pristine NaCl shows no emission under 254 nm UV lamp, however, they display green luminescence after doping, as shown in Fig. 2a. This is because the incorporation of Sb^{3+} leads to the formation of Sb–Cl clusters as emissive centers and introduces impurity states, resulting in luminescence.[21,30] To understand their luminescence mechanism and photophysical processes, photoluminescence (PL) spectra were studied in detail. When excited at 320 nm, NaCl:Sb^{3+} exhibits a broad green emission with a PL peak at 536 nm and a full-width at half maximum (FWHM) of 121 nm (Fig. 2b). The PL excitation (PLE) peak of NaCl:Sb^{3+} is at 312 nm and originates from the contributions of Sb^{3+} orbitals, indicating a large Stokes shift of 224 nm. To demonstrate the feasibility of this doping strategy for other alkali halides, we also explored the replacement of NaCl with KCl and RbCl in the precursor while maintaining an Sb^{3+} concentration of 30%. The successful incorporation of Sb^{3+} into KCl and RbCl SCs was confirmed by their PXRD patterns, which are in good agreement with the standard XRD patterns (Fig. 1). Additionally, SEM-EDS measurements demonstrate the presence and uniform distribution of the elements (Fig. S2 and S3, ESI†). The emission peak red-shifts to 567 nm and 574 nm when the alkali metal is changed from Na to K and Rb, respectively, whereas the PLE peaks of Sb-doped KCl and RbCl are located at 302 nm and 320 nm, respectively. The PL peak shift indicates that the radius and electron density of the alkali ion affect the location and concentration of Sb^{3+} dopants in the host crystals, significantly impacting the band structures and resulting in different optical properties.[31] A similar red-shift in PL has also been observed in the all-inorganic blue-emissive A_2CuX_3 (A = K, Rb; X = Cl, Br) and Sb^{3+}-doped Cs_2MInCl_6 (M = Ag, K, and Na) single crystals when using the alkali metal with larger radius due to a greater degree of Jahn–Teller distortion.[32,33] The highest photoluminescence quantum yield (PLQY) for these samples was approximately 1.5%, observed in NaCl:Sb^{3+}.

Time-resolved PL (TRPL) measurements were conducted to gain deeper insights into the optical properties of these materials. As shown in Fig. 2c and 3a, the PL decay curve of NaCl:Sb^{3+} exhibits both fast and slow decay components. To determine the lifetime of the fast decay, we used a shorter time scale of 10 ns to measure the same spot on the sample (Fig. S4, ESI†). By using bi-exponential function fitting method, a short lifetime of 2.7 ns and a long lifetime of 1.5 μs are obtained. Similarly, KCl:Sb^{3+} exhibits a short lifetime of 2.3 ns and a long lifetime of 2.4 μs, while RbCl:Sb^{3+} shows a short lifetime of 3.3 ns and a long lifetime of 2.6 μs. The broadband

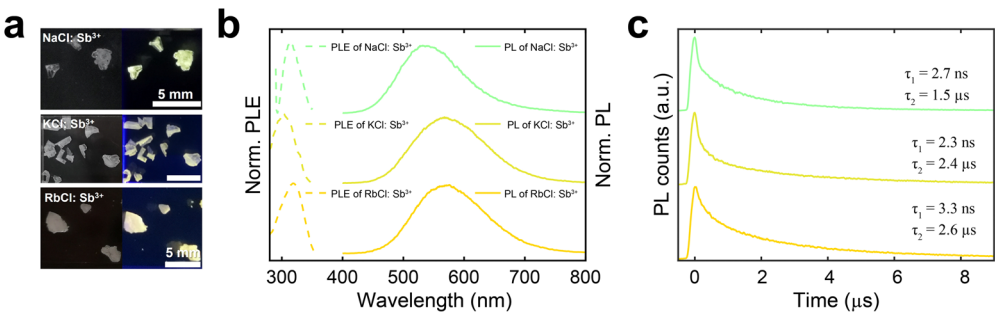

Fig. 2 (a) Optical images of Sb^{3+}-doped ACl (A = Na, K, and Rb) single crystals under ambient and UV light (254 nm). (b) Solid lines: PL emission spectra of Sb^{3+}-doped ACl (A = Na, K, and Rb). Dashed lines: PLE spectra of the same materials. (c) Time-resolved PL decay curves of Sb^{3+}-doped ACl (A = Na, K, and Rb) single crystals.

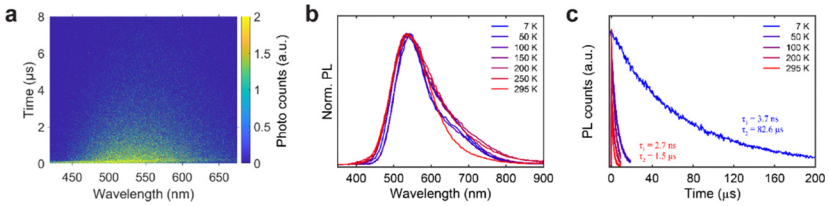

Fig. 3 (a) TRPL 2D mapping of NaCl:Sb^{3+} measured at room temperature. Temperature-dependent (b) PL and (c) TRPL decays of NaCl:Sb^{3+} measured from 7 to 295 K. The lifetime values shown in (c) are associated with temperatures at 7 K (blue) and 295 K (red).

PL spectra and microsecond PL lifetimes of these compounds suggest that their emissions likely originate from self-trapped excitons (STEs) due to the introduction of Sb^{3+}, a phenomenon commonly observed in Sb^{3+}-doped metal halides.[23,30,34–36] The fast and slow components of the emission can be attributed to the singlet and triplet states of the STE transitions of the ns^2 emission centers from Sb^{3+}, respectively.[37–40] STEs are found in materials with soft lattices and strong exciton–phonon coupling.[41] The STE property is profoundly influenced by inorganic structure distortion.[42] Upon photogeneration, the Sb–Cl clusters become distorted, causing excitons to quickly self-trap and form singlet STEs due to their lower energy. Some of these excitons relax to the ground state, while others tend to undergo an intersystem crossing (ISC) process from singlet STEs to triplet STEs. Ultimately, the broad emission with a large Stokes shift is attributed to the recombination of triplet STEs back to the ground state.[41,43] We anticipate that larger alkali metal ions make the crystal lattice more prone to distortion, which facilitates the formation of STEs and enhances the localization of excitons within the lattice. Localized excitons typically exhibit a lower non-radiative recombination rate, thereby extending the emission lifetime.

Temperature-dependent PL and TRPL measurements are performed to further demonstrate the STEs emission property of ACl:Sb^{3+} (A = Na, K, and Rb) SCs over a temperature range of 7 to 295 K. As shown in Fig. 3b, the maximum emission peak at 536 nm shows no obvious changes despite variations in temperature. However, the PL of NaCl:Sb^{3+} exhibits a longer tail and an additional band around 680 nm when the temperature decreases. Moreover, its lifetime (Fig. 3c and Fig. S11, ESI†) increases significantly, with τ_1 rising from 2.7 to 3.7 ns and τ_2 from 1.5 to 82.6 μs, as the temperature decreases from 295 K to 7 K. These changes can be attributed to suppressed non-radiative recombination and reduced thermal quenching resulting from the thermal dissociation of excitons.[44] The PL peak of KCl:Sb^{3+} shifts from 567 to 585 nm when the temperature decreased from 295 K to 7 K (Fig. S9, ESI†). This red-shift may be due to changes in the electronic band structure caused by thermal contraction and enhanced electron–phonon interaction and localization of STEs at lower temperature.[45–48] Similar to the Sb^{3+}-doped NaCl counterpart, the lifetimes of both KCl:Sb^{3+} and RbCl:Sb^{3+} at 7 K are much longer than those at 295 K (Fig. S12–S15, ESI†). For KCl:Sb^{3+}, τ_1 increases from 2.3 to 3.7 ns, and τ_2 increases from 2.4 to 21.3 μs. As for RbCl:Sb^{3+}, the lifetime of fast component shows no significant change, while the lifetime of slow component increases from 2.6 to 27.5 μs.

We also investigated the effect of Sb^{3+} dopant concentration on NaCl:Sb^{3+}. As shown in the Fig. S16 (ESI†), the PXRD peaks do not display an obvious shift or any impurity phase with increasing Sb^{3+} doping levels, and the crystal cell-volume shows minimal variation (Table S1, ESI†). This suggests a low dopant concentration and that the dopants do not alter the crystal structure, which can be attributed to the size difference of Na and Sb and the impurity ion lattice solubility. To confirm actual Sb doping levels in NaCl, we conducted EDS measurements (Table S2, ESI†). As the Sb content increases, the measured dopant ratios are notably lower than the nominal values, suggesting a limited solubility of Sb in NaCl. These low doping levels are consistent with the PXRD results. Furthermore, their PL spectra (Fig. S18, ESI†) show no significant change with different doping ratios, indicating that the Sb doping concentration does not substantially affect the exciton binding energy in the system, and the excitons are highly localized around the Sb ions.[49,50]

In conclusion, we synthesized a family of Sb^{3+}-doped ACl (A = Na, K, and Rb) single crystals exhibiting green to yellow emission with PL peaks ranging from 536 to 574 nm. Their broad spectra, large Stokes shifts and long lifetimes can be attributed to STE emissions. The PL peak red-shifted with the increasing radius of alkali metals, which is related to lattice distortion. These non-toxic luminescent compounds may have potential applications in lighting and displays. Moreover, this simple and versatile method for tuning the emissive features of metal halides may lay the foundation for the synthesis and research of new lead-free metal halides.

This research was supported by Grant 2022066 from the United States-Israel Binational Science Foundation (BSF). This research used resources (Advanced Optical Spectroscopy) of the Center for Functional Nanomaterials (CFN), which is a U.S. Department of Energy Office of Science User Facility, at Brookhaven National Laboratory under Contract No. DE-SC0012704. Work performed at the Center for Nanoscale Materials, a U.S. Department of Energy Office of Science User Facility, was supported by the U.S. DOE, Office of Basic Energy Sciences, under Contract No. DE-AC02-06CH11357. We thank B. T. Diroll for help with PLQY experiments.

Data availability

The data supporting this article have been included as part of the ESI.†

Conflicts of interest

There are no conflicts to declare.

Notes and references

1 X.-K. Liu, W. Xu, S. Bai, Y. Jin, J. Wang, R. H. Friend and F. Gao, *Nat. Mater.*, 2021, **20**, 10–21.
2 M. Worku, A. Ben-Akacha, T. Blessed Shonde, H. Liu and B. Ma, *Small Sci.*, 2021, **1**, 2000072.
3 J. S. Kim, J.-M. Heo, G.-S. Park, S.-J. Woo, C. Cho, H. J. Yun, D.-H. Kim, J. Park, S.-C. Lee and S.-H. Park, *Nature*, 2022, **611**, 688–694.
4 A. Ho-Baillie, M. Zhang, C. F. J. Lau, F.-J. Ma and S. Huang, *Joule*, 2019, **3**, 938–955.
5 W. Xiang and W. Tress, *Adv. Mater.*, 2019, **31**, 1902851.
6 M. Pitaro, E. K. Tekelenburg, S. Shao and M. A. Loi, *Adv. Mater.*, 2022, **34**, 2105844.
7 H. P. Wang, S. Li, X. Liu, Z. Shi, X. Fang and J. H. He, *Adv. Mater.*, 2021, **33**, 2003309.
8 J. Lv, X. Lu, X. Li, M. Xu, J. Zhong, X. Zheng, Y. Shi, X. Zhang and Q. Zhang, *Small*, 2022, **18**, 2201715.
9 P. Ran, L. Yang, T. Jiang, X. Xu, J. Hui, Y. Su, C. Kuang, X. Liu and Y. Yang, *Adv. Mater.*, 2022, **34**, 2205458.
10 Q. Guo, X. Zhao, B. Song, J. Luo and J. Tang, *Adv. Mater.*, 2022, 2201008.
11 T. C. Jellicoe, J. M. Richter, H. F. Glass, M. Tabachnyk, R. Brady, S. E. Dutton, A. Rao, R. H. Friend, D. Credgington and N. C. Greenham, *J. Am. Chem. Soc.*, 2016, **138**, 2941–2944.
12 M.-G. Ju, J. Dai, L. Ma and X. C. Zeng, *J. Am. Chem. Soc.*, 2017, **139**, 8038–8043.
13 B. Yang, J. Chen, F. Hong, X. Mao, K. Zheng, S. Yang, Y. Li, T. Pullerits, W. Deng and K. Han, *Angew. Chem., Int. Ed.*, 2017, **56**, 12471–12475.
14 J. Zhang, Y. Yang, H. Deng, U. Farooq, X. Yang, J. Khan, J. Tang and H. Song, *ACS Nano*, 2017, **11**, 9294–9302.
15 N. K. Tailor, A. Listorti, S. Colella and S. Satapathi, *Adv. Mater. Technol.*, 2023, **8**, 2200442.
16 Y. Li, Z. Zhou, N. Tewari, M. Ng, P. Geng, D. Chen, P. K. Ko, M. Qammar, L. Guo and J. E. Halpert, *Mater. Chem. Front.*, 2021, **5**, 4796–4820.
17 Z. Yang, Z. Jiang, X. Liu, X. Zhou, J. Zhang and W. Li, *Adv. Opt. Mater.*, 2019, **7**, 1900108.
18 Y. Jing, Y. Liu, X. Jiang, M. S. Molokeev, Z. Lin and Z. Xia, *Chem. Mater.*, 2020, **32**, 5327–5334.
19 A. K. Guria, S. K. Dutta, S. D. Adhikari and N. Pradhan, *ACS Energy Lett.*, 2017, **2**, 1014–1021.
20 C. M. Shi, H. L. Xuan, Y. Wu, L. J. Xu and Z. N. Chen, *Adv. Opt. Mater.*, 2022, 2202376.
21 J. Wu, X. Li, X. Lian, B. Su, J. Pang, M.-D. Li, Z. Xia, J. Z. Zhang, B. Luo and X.-C. Huang, *ACS Nano*, 2021, **15**, 15354–15361.
22 T. Chang, H. Wang, Y. Gao, S. Cao, J. Zhao, B. Zou and R. Zeng, *Inorg. Chem.*, 2022, **61**, 1486–1494.
23 J. Jin, Y. Peng, Y. Xu, K. Han, A. Zhang, X.-B. Yang and Z. Xia, *Chem. Mater.*, 2022, **34**, 5717–5725.
24 Y. Rodriguez-Lazcano, V. Correcher and J. Garcia-Guinea, *Radiat. Phys. Chem.*, 2012, **81**, 126–130.
25 S. Sabharwal, S. Kathuria and B. Ghosh, *Nucl. Instrum. Methods Phys. Res., Sect. A*, 1987, **255**, 501–506.
26 P. Sibczyński, M. Moszyński, T. Szczęśniak, W. Czarnacki, A. Syntfeld-Każuch and P. Schotanus, *NSS/MIC*, 2010, pp. 574–579.
27 Y. Li, Y. Li, C. Li, X. Zhang, F. Zeng, H. Lin, Z. Su and C. Mahadevan, *J. Alloys Compd.*, 2020, **849**, 156592.
28 J. Pascual, L. Arizmendi, F. Jaque and F. Agulló-López, *J. Lumin.*, 1978, **17**, 325–343.
29 S. Radharkishna and A. Karguppikar, *J. Phys. Chem. Solids*, 1973, **34**, 1497–1505.
30 I. A. de Carcer, F. Cussó, F. Jaque, E. Espana, T. Calderon, G. Lifante and P. Townsend, *J. Phys. D: Appl. Phys.*, 1993, **26**, 154.
31 Y. Zhang, X. Liu, H. Sun, J. Zhang, X. Gao, C. Yang, Q. Li, H. Jiang, J. Wang and D. Xu, *Angew. Chem., Int. Ed.*, 2021, **60**, 7587–7592.
32 Y. Li, Z. Zhou, F. K. Sheong, Z. Xing, K. S. Wong, H. H. Sung, I. D. Williams and J. E. Halpert, *Chem. Mater.*, 2023, **35**, 1318–1324.
33 Z. Zhou, Y. Li, Z. Xing, Z. Li, K. S. Wong and J. E. Halpert, *ACS Appl. Nano Mater.*, 2021, **4**, 14188–14196.
34 C. Zhao, Y. Gao and J. Qiu, *ACS Appl. Mater. Interfaces*, 2023, **15**, 59610–59617.
35 X. Mao, Z. Wang, F. Zhang, H. Yin, X. Xu, J. Chen, Z. Chen, J. Luo, K. Han and R. Zhang, *J. Phys. Chem. Lett.*, 2023, **14**, 1521–1527.
36 K. M. McCall, V. Morad, B. M. Benin and M. V. Kovalenko, *ACS Mater. Lett.*, 2020, **2**, 1218–1232.
37 Z. Li, Y. Li, P. Liang, T. Zhou, L. Wang and R.-J. Xie, *Chem. Mater.*, 2019, **31**, 9363–9371.
38 J. Huang, T. Chang, R. Zeng, J. Yan, Q. Wei, W. Zhou, S. Cao and B. Zou, *Adv. Opt. Mater.*, 2021, **9**, 2002267.
39 P. Han, C. Luo, S. Yang, Y. Yang, W. Deng and K. Han, *Angew. Chem., Int. Ed.*, 2020, **132**, 12809–12813.
40 L. Zhou, J. F. Liao, Z. G. Huang, J. H. Wei, X. D. Wang, H. Y. Chen and D. B. Kuang, *Angew. Chem., Int. Ed.*, 2019, **131**, 15581–15586.
41 R. Zhang, X. Mao, Y. Yang, S. Yang, W. Zhao, T. Wumaier, D. Wei, W. Deng and K. Han, *Angew. Chem., Int. Ed.*, 2019, **58**, 2725–2729.
42 Q. Guo, X. Zhao, B. Song, J. Luo and J. Tang, *Adv. Mater.*, 2022, **34**, 2201008.
43 S. Li, J. Luo, J. Liu and J. Tang, *J. Phys. Chem. Lett.*, 2019, **10**, 1999–2007.
44 Y. Jing, Y. Liu, J. Zhao and Z. Xia, *J. Phys. Chem. Lett.*, 2019, **10**, 7439–7444.
45 B. Su, M. Li, E. Song and Z. Xia, *Adv. Funct. Mater.*, 2021, **31**, 2105316.
46 R. Lin, Q. Guo, Q. Zhu, Y. Zhu, W. Zheng and F. Huang, *Adv. Mater.*, 2019, **31**, 1905079.
47 B. J. Foley, D. L. Marlowe, K. Sun, W. A. Saidi, L. Scudiero, M. C. Gupta and J. J. Choi, *Appl. Phys. Lett.*, 2015, **106**, 243904.
48 W. A. Saidi, S. Poncé and B. Monserrat, *J. Phys. Chem. Lett.*, 2016, **7**, 5247–5252.
49 B. Su, J. Jin, K. Han and Z. Xia, *Adv. Funct. Mater.*, 2023, **33**, 2210735.
50 X. Meng, Q. Wei, W. Lin, T. Huang, S. Ge, Z. Yu and B. Zou, *Inorg. Chem.*, 2022, **61**, 7143–7152.